2011-12

Dissecting the structure, thermodynamic stability, and aggregation properties of the A25T transthyretin (A25T-TTR) variant involved in leptomeningeal amyloidosis: identifying protein partners that co-aggregate during A25T-TTR fibrillogenesis in cerebrospinal fluid

Biochemistry, Washington, DC : American Chemical Society - ACS, v. 50, n. 51, p. 11070-11083, Dec. 2011

BIOCHEMISTRY
including biophysical chemistry & molecular biology

Article

pubs.acs.org/biochemistry

Dissecting the Structure, Thermodynamic Stability, and Aggregation Properties of the A25T Transthyretin (A25T-TTR) Variant Involved in Leptomeningeal Amyloidosis: Identifying Protein Partners That Co-Aggregate during A25T-TTR Fibrillogenesis in Cerebrospinal Fluid

Estefania P. C. Azevedo,[†] Humberto M. Pereira,[‡] Richard C. Garratt,[‡] Jeffery W. Kelly,[§] Debora Foguel,*[,†] and Fernando L. Palhano*[,†,§]

[†]Instituto de Bioquímica Médica, Programa de Biologia Estrutural, Universidade Federal do Rio de Janeiro, Rio de Janeiro, 21941-590 Brazil

[‡]Centro de Biotecnologia Molecular Estrutural, Instituto de Física de São Carlos, Universidade de São Paulo, São Paulo, 13560-970 Brazil

[§]Departments of Chemistry and Molecular and Experimental Medicine and Skaggs Institute for Chemical Biology, The Scripps Research Institute, La Jolla, California 92037, United States

Supporting Information

ABSTRACT: Deposition of amorphous aggregates and fibrils of transthyretin (TTR) in leptomeninges and subarachnoid vessels is a characteristic of leptomeningeal amyloidosis (LA), a currently untreatable cerebral angiopathy. Herein, we report the X-ray structure of the A25T homotetramer of TTR, a natural mutant described in a patient with LA. The structure of A25T-TTR is indistinguishable from that of wild-type TTR (wt-TTR), indicating that the difference in amyloidogenicity between A25T-TTR and wt-TTR cannot be ascribed to gross structural differences. Using pressure-induced dissociation of the tetramer, we show that A25T-TTR is 3 kcal/mol less stable than L55P-TTR, the most aggressive mutant of TTR described to date. After incubation for 15 days at 37 °C (pH 7.3), A25T-TTR forms mature amyloid fibrils. To mimic the environment in which TTR aggregates, we investigated aggregation in cerebrospinal fluid (CSF). Unlike L55P-TTR, A25T-TTR rapidly forms amyloid aggregates in CSF that incorporated several protein partners. Utilizing a proteomics methodology, we identified 19 proteins that copurified with A25T-TTR amyloid fibrils. We confirmed the presence of proteins previously identified to be associated with TTR aggregates in biopsies of TTR amyloidosis patients, such as clusterin, apolipoprotein E, and complement proteins. Moreover, we identified novel proteins, such as blood coagulation proteins. Overall, our results revealed the in vitro characterization of TTR aggregation in a biologically relevant environment, opening new avenues of investigation into the molecular mechanisms of LA.

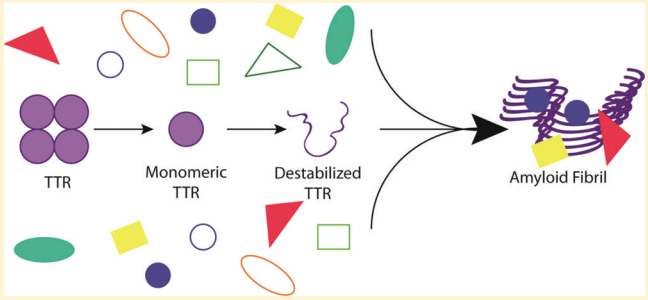

Protein misfolding diseases include a broad range of pathologies in which proteins fail to fold properly and are degraded or cease to remain in their folded state once folded, populating partially denatured states.[1] At sufficient concentrations, partially denatured states can lead to protein aggregation, resulting in a spectrum of quaternary structures, including oligomers, protofibrils, and fibrils.[2] Many degenerative diseases are associated with protein cross-β-sheet quaternary structure, or amyloid fibril, formation termed the amyloidoses.[3] Amyloid deposits can be detected using Congo red birefringence or thioflavin T fluorescence and are often associated with glycosaminoglycans, the amyloid P component, and other proteins. Amyloid filaments often share an in-register parallel cross-β quaternary structure in which the strands are oriented perpendicular to the fibril axis. Amyloid fibrils usually consist of multiple interacting filaments that are at least two β-sheets thick.[4−6] Some fibrils are formed by a highly ordered triangular core, which is in turn formed by three parallel cross-β sheets.[7] On the basis of the generic nature of these assemblies, it has been proposed that any protein, regardless of its amino acid sequence, can form amyloid fibrils if subjected to appropriate solution conditions.[8,9]

Transthyretin (TTR) is a 54 kDa homotetrameric protein composed of identical 127-residue subunits exhibiting a predominantly β-sheet tertiary structure.[10] TTR is secreted into the human bloodstream by the liver and into the cerebrospinal fluid (CSF) by the choroid plexus. Each TTR monomer is composed of one α-helix and eight β-strands

Received: August 29, 2011
Revised: November 3, 2011
Published: November 17, 2011

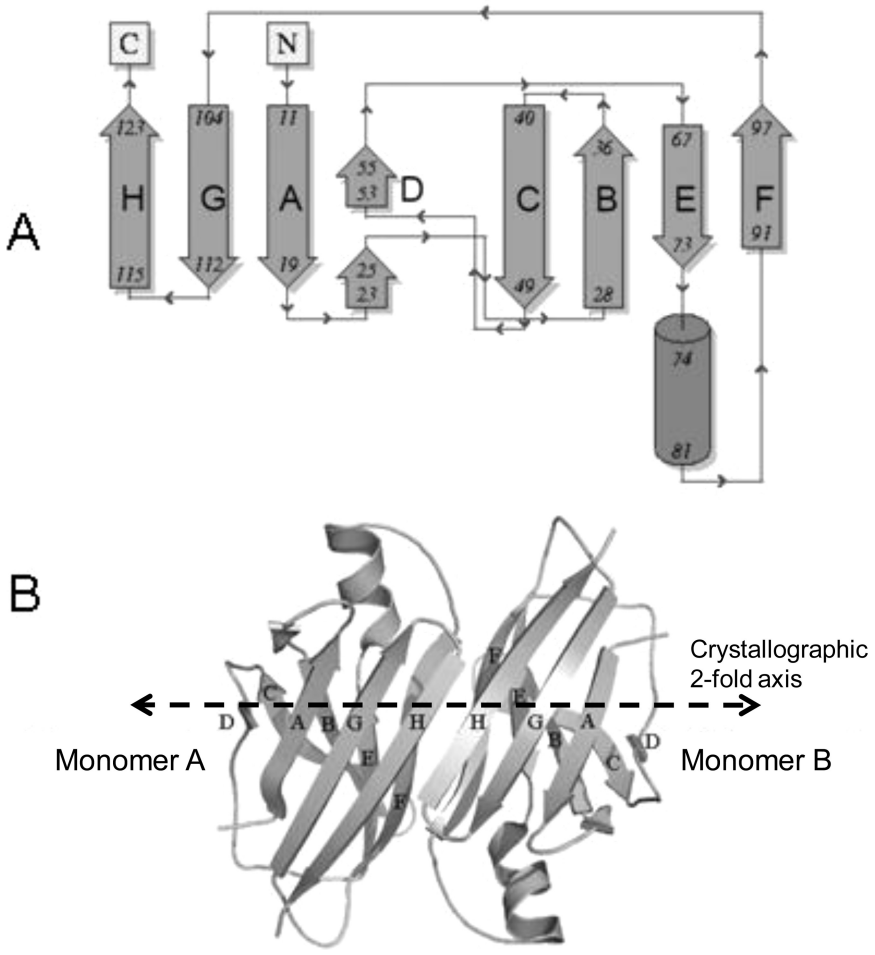

Figure 1. Ribbon diagram of transthyretin (TTR). (A) Schematic representation of the secondary structure of TTR generated using PDBsum, where β-strands A–H are represented by arrows and the α-helix is represented by a cylinder. C and N represent the C- and N-termini of the protein, respectively. (B) Schematic representation of the TTR dimer composed of monomers A and B with the two β-sheets (DAGH and CBEF) represented in each monomer.

(denoted A–H) arranged in a characteristic sandwich of two β-sheets [DAGH and CBEF (Figure 1)]. The dimer (AB) is held together by antiparallel β-sheet hydrogen bonds and hydrophobic side chain–side chain interactions involving the H strands located along the edge of each monomer. Two dimers (AB and CD) associate back to back via hydrophobic interactions involving residues of the loops that connect strands AB and GH, creating the less stable dimer–dimer interface.[11]

In the blood, TTR serves as a tertiary carrier for thyroxine (T4), and as such, 99% of its binding sites are unoccupied. TTR binds to and carries ~0.5 equiv of retinol-binding protein in the blood.[12] In the CSF, TTR is the primary T4 transporter.[13] Secreted TTR can form amyloid fibrils in the extracellular space, leading to various amyloid-related pathologies. The amyloidogenesis of wild-type TTR (wt-TTR) leads to senile systemic amyloidosis, a cardiomyopathy that affects 10–25% of people more than 70 years of age and is characterized by heavy amyloid deposits in the heart.[14] The amyloidogenesis of more than 80 point mutations of TTR appears to cause familial amyloidotic polyneuropathy (FAP) and/or familial amyloidotic cardiomyopathy (FAC), or central nervous system amyloidosis (CNSA).[15] Among the variants of TTR, the V30M and V122I (3% of people of African descent have this mutation) TTR mutations are the clinically most important because of their high frequency of occurrence in causing FAP and FAC, respectively. On the other hand, A25T is one of rare TTR mutations associated with an amyloidosis that is restricted to the central nervous system (CNS) and is characterized by the deposition of amyloid fibrils in the leptomeningeal and subarachnoid vessels.[16] Sekijima and coworkers[16] have described tetramers composed of this mutant subunit as being highly unstable. Although tetramer instability is positively correlated with pathology severity and onset,[17−20] A25T-related amyloidosis has a late onset and is peculiar in that it does not result in a peripheral amyloid disease, only a brain disease. Because of the instability of the A25T-TTR tetramer, this protein is detected as being misfolded in the endoplasmic reticulum of liver cells and is largely degraded by the proteasome instead of being secreted into the bloodstream. The high concentration of T4 in the choroid plexus serves as a pharmacologic chaperone enhancing TTR tetramer folding efficiency in the endoplasmic reticulum, leading to secretion of the A25T subunit-containing TTR tetramer.[20] After secretion, the T4 no longer binds, allowing dissociation of the tetramer and subsequent A25T TTR amyloidogenesis.

Several hypotheses have been proposed to explain the amyloidogenic properties of TTR. The hypothesis consistent with all the data posits the dissociation of the tetramer into a monomeric, partially unfolded state, which aggregates by a

thermodynamically favorable misassembly process (nucleation not required).[2,21−25] Investigations have shown that disruption of β-strands C and D may expose hydrophobic regions of the protein to solvent, leading to aggregation.[26−28] Recently, we have shown that TTR has three canonical Zn^{2+}-binding sites.[29] Zn^{2+} binding induces structural perturbations that lead to TTR aggregation.[29,30] Most studies have used acidic pH to induce TTR aggregation[16,18] in vitro. However, it is still unknown whether TTR is exposed to acidic environments during its lifetime[23] or how the tetramer dissociation and partial monomer unfolding required for amyloidogenesis occur in vivo. Thus, ex vivo studies mimicking in vivo conditions are required for an improved understanding of the mechanisms behind TTR aggregation to define possible targets for effective therapies against TTR-related amyloidosis.[31]

Currently, FAP patients are treated by liver transplant, in which a patient's liver expressing a TTR variant, typically V30M, is replaced by one that expresses the wt protein. Although liver transplantation retards the progression of FAP, it does not eliminate aggregates that have already been deposited.[32] Moreover, many FAP patients later develop cardiomyopathy from deposition of wt-TTR on top of prior deposition of V30M. There is, however, no treatment for patients bearing CNSA-related TTR mutations, and surprisingly, liver transplantation does not seem to be effective for all disease-associated variants.[33−35]

Many studies have focused on developing effective and selective TTR ligands that can prevent TTR dissociation and aggregation.[36−39] Nonsteroidal anti-inflammatory drugs (NSAIDs) have been described as effective stabilizers of TTR tetramers,[40] and most recently, the Committee for Medicinal Products for Human Use recommended the granting of a marketing authorization for the drug Vyndaqel (tafamidis) for the treatment of FAP patients (http://www.ema.europa.eu).

In this study, we investigated one of the variants whose amyloidogenesis leads to CNSA, A25T-TTR. The X-ray structure of the A25T-TTR homotetramer was determined to 2.03 Å resolution. In keeping with all of the amyloid disease-associated TTR mutants studied to date, the structure of A25T-TTR showed no profound alterations relative to the wt-TTR structure. Through the use of high hydrostatic pressure, we were able to assess the thermodynamic parameters (ΔG_a and ΔV_a) of A25T-TTR folding and association, and we showed that A25T-TTR is less stable than one of the most destabilized variants, L55P-TTR, that leads to very early onset polyneuropathy. Utilizing an array of techniques, we analyzed the A25T-TTR aggregation kinetics in buffer at pH 7.3, as well as in CSF, the environment in which it aggregates in vivo. Interestingly, the amyloid fibrils formed in CSF were composed of several other proteins besides TTR that are present in this complex physiological environment.

EXPERIMENTAL PROCEDURES

Expression and Purification of Recombinant TTR. The expression and purification of recombinant wt-TTR and the A25T-TTR and L55P-TTR mutants were performed as previously described.[41] For the A25T-TTR variant, the 30 min incubation at 60 °C[41] was omitted because of the instability of this protein. The protein concentration was measured and calculated using an extinction coefficient of 7.76×10^4 M^{-1} cm^{-1} at 280 nm.

Spectroscopic Measurements under High Hydrostatic Pressure (HHP). HHP has been described elsewhere as an effective tool for the study of protein folding and oligomerization.[42] We used a high-pressure cell equipped with optical windows[43] (ISS Inc., Champaign, IL). Fluorescence spectra were recorded on an ISS K2 spectrofluorimeter (ISS Inc.). In all experiments, protein was diluted in buffer containing 25 mM Tris-HCl, 50 mM KCl, and 1 mM EDTA (pH 7.5), and the pressure was increased in steps of 200 bar. At each step, the sample was allowed to equilibrate for 20 min prior to measurements, and protein denaturation was monitored using the tryptophan emission spectra. The mean energy of the fluorescence emission was evaluated by calculating the center of spectral mass $\langle \nu_p \rangle$ at pressure p:

$$\left\langle \nu_p \right\rangle = \sum \nu_i F_i / \sum F_i \quad (1)$$

where F_i is the fluorescence emitted at wavelength ν_i. The degree of dissociation (α) is related to $\langle \nu_p \rangle$ by the expression

$$a = (\left\langle \nu_p \right\rangle - \left\langle \nu_i \right\rangle)/(\left\langle \nu_i \right\rangle - \left\langle \nu_f \right\rangle) \quad (2)$$

where $\langle \nu_i \rangle$ and $\langle \nu_f \rangle$ are the initial and final values of the center of spectral mass, respectively, in nanometers.

We noted that the initial center of spectral mass values for all proteins used in HHP assays were recovered after decompression.

Thermodynamic Parameters. The standard volume changes upon folding (ΔV_a) for the A25T-TTR and L55P-TTR mutants and the equilibrium dissociation constants (K_d) were determined using the thermodynamic relation

$$\ln[a_p{}^4/(1 - a_p)] = p(\Delta V/RT) + \ln(K_d/256C^3) \quad (3)$$

This equation permits the calculation of the standard volume change, ΔV_a, for a tetramer ↔ monomer equilibrium from measurements at a fixed protein concentration C at different pressures. A change in protein concentration from C_1 to C_2 at a fixed pressure results in a parallel displacement (Δp) of the plot of $\ln[\alpha_p{}^4/(1 - \alpha_p)]$ versus p. At 50% dissociation, this shift ($\Delta p_{1/2}$) in pressure with the change in concentration is given by eq 4, which allows the determination of the half-maximal pressure capable of dissociating each protein concentration under a given condition:[17]

$$\Delta p_{1/2} = (n - 1)(RT/\Delta V) \ln(C_2/C_1) \quad (4)$$

Crystallization, Data Collection, and Structure Refinement of A25T-TTR. A25T-TTR was crystallized by hanging-drop vapor diffusion. Crystals were grown for 1 week at 20 °C in buffer containing 100 mM HEPES, 200 mM $CaCl_2$, and 28% PEG400 (pH 7.5) via equilibration of 1 μL of 10 mg/mL TTR with 1 μL of buffer solution. The A25T-TTR X-ray diffraction data were collected using a home source (Rigaku Micromax 007HF with Varimax HF mirrors and an RAXIS IV^{++} IP detector employing Cu Kα radiation; λ = 1.5418 Å) (Table 1). The data were collected at 100 K using 1° oscillations per image for a total of 100 images. The diffraction data were processed using XDS[44] up to 2.05 Å resolution. The structure of A25T-TTR was determined by molecular replacement with Phaser[45] using the apo form of human TTR as a search model (Protein Data Bank entry 3CFM). The refinement was performed using Phenix[46] and Coot.[47] The electron density for the A25T-TTR mutation was clearly identifiable, allowing the correct positioning of the T25 side chain. Validation of the

Table 1. Full Data Collection and Refinement Statistics for A25T-TTR

Data Collection	
space group	$P2_12_12$
cell dimensions *a*, *b*, *c* (Å)	43.08, 64.17, 85.55
detector	RAXIS IV^{++}
X-ray source	Rigaku MicroMax007 VarimaxHF
wavelength (Å)	1.5418
resolution range (Å)	20.0−2.03 (2.15−2.03)
redundancy	3.77 (3.5)
R_{meas} (%)	11.4 (72.0)
completeness (%)	98.7 (94.6)
total no. of reflections	59145(8258)
no. of unique reflections	15676 (2494)
$I/\sigma(I)$	9.94 (2.22)
Refinement	
no. of reflections used for refinement	15663
R (%)	19.12
R_{free} (%)	23.94
overall averaged B factor (Å^2)	35.70
no. of protein atoms	1797
no. of water molecules	167
Ramachandran plot	
favored region (%)	99.5
outliers (%)	0.5
rmsd from ideal geometry	
bond lengths (Å)	0.004
bond angles (deg)	0.668

structural model was performed with Procheck[48] and Molprobity.[49]

Size-Exclusion Chromatography. The formation of aggregates was monitored by size-exclusion chromatography on a GPC 300 column (SynChropak) coupled to a high-performance liquid chromatography system (Shimadzu SPD-10A). The system was equilibrated in buffer containing 25 mM Tris-HCl, 50 mM KCl, and 1 mM EDTA (pH 7.3) at a flow rate of 0.4 mL/min. Protein samples were prepared in PBS and aged at 37 °C for 20 days. Samples were withdrawn at different times for size-exclusion gel filtration chromatography, and sample elution was monitored by tryptophan fluorescence at 330 nm and absorbance at 280 nm. The peak areas for the estimated tetramer elution volume and the aggregate elution volume were calculated.

Congo Red and Thioflavin T Binding Assays. Fibril formation was assessed using Congo red and thioflavin T (thio-T) binding assays. Congo red binding was analyzed using fluorescence microscopy in a Nikon TE 3000 microscope (Zeiss). The samples were pelleted and resuspended in 5 mM potassium phosphate and 150 mM NaCl (pH 7.4) containing 10 μM Congo red. A small amount was dropped onto a glass slide and analyzed. For thio-T binding assays, fibril pellets were diluted to 45 μg/mL in 5 mM potassium phosphate and 150 mM NaCl (pH 7.4) containing 20 μM thio-T, and binding was monitored using a spectrofluorimeter to measure the fluorescence increase (excitation at 450 nm and fluorescence emission at 465−520 nm).

Western Blot and Dot-Blot Assays. Samples of wt-TTR and the A25T-TTR and L55P-TTR variants, at a concentration of 3.5 μM, were incubated for 11 days at 37 °C in phosphate buffer (pH 7.3) (PBS). Aliquots were adsorbed on a PVDF membrane that had been previously washed in methanol. Membranes were blocked with 5% skim milk, washed with Tris-buffered saline containing 0.05% Tween 20 (pH 7.5) (TTBS), and incubated overnight at 4 °C with the A11 antibody (1:5000)[50] or a rabbit polyclonal anti-TTR antibody (1:10000) (Dako, Carpinteria, CA). Membranes were then washed thoroughly with TTBS and incubated with goat polyclonal anti-rabbit IgG conjugated to horseradish peroxidase (1:10000). Samples were visualized using an ECLplus kit (GE Healthcare).

Aggregation of TTR in Human CSF. Aggregation was performed via incubation of 3.5 μM A25T-TTR or L55P-TTR in PBS or human CSF (Biochemed Services, Winchester, VA) containing 5 mM NaN_3 for 15 days at 37 °C. Samples were taken daily, diluted 10-fold, and submitted to 12% native PAGE at 4 °C and 100 V. The samples were transferred to PVDF membranes, and Western blotting was performed as described above. The bands were quantified using ImageJ. The fraction of remaining tetramers was calculated from the native PAGE analysis by dividing the area of the remaining tetramer by the area of the tetramer on the first day of the kinetic analysis.

Electron Microscopy (EM). After aggregation for 15 days in PBS or CSF, the samples were centrifuged at 16000*g* for 30 min at 4 °C to obtain insoluble fractions. These aggregates were washed twice with PBS and resuspended in ddH_2O, yielding 45 μg/mL protein. Copper grids (carbon- and Formvar-coated 400 mesh) (Electron Microscopy Sciences, Hatfield, PA) were glow-discharged and inverted on a 5 μL aliquot of sample for 3 min. Excess sample was removed, and the grids were immediately placed briefly on a droplet of doubly distilled water followed by a 2% uranyl acetate solution for 2 min. Excess stain was removed and the grid allowed to dry thoroughly. Grids were then examined on a Philips CM100 electron microscope (FEI, Hillsbrough, OR) at 80 kV and images collected using a Megaview III ccd camera (Olympus Soft Imaging Solutions, Lakewood, CO).

Analyses of Proteins that Co-Aggregate with A25T-TTR Fibrils. A25T-TTR aggregates were obtained from A25T-TTR (3.5 μM) aged for 15 days at 37 °C in PBS or human CSF containing 5 mM NaN_3. The samples were centrifuged at 16000*g* for 30 min at 4 °C to yield insoluble fractions. These aggregates were washed twice with PBS and resuspended in PBS, and the protein concentration was determined using bicinchoninic acid reagent. As a control, we incubated human CSF with 3.5 μM recombinant wt-TTR under the same conditions. In this case, no aggregated material was observed. The samples were separated by 4 to 12% SDS−PAGE and stained with Coomassie blue G 250 or submitted to proteomics analysis. For proteomics study, the samples were treated with Rapigest (Waters), reduced with 200 mM DTT, alkylated with 200 mM iodoacetamide, and digested with trypsin overnight using an estimated 1:30 enzyme:substrate ratio. One-dimensional liquid chromatography and mass spectrometry (LC−MS/MS) was performed on an Agilent q-TOF mass spectrometer as described previously.[51] The proteomic data analysis was performed using the NCBInr database as described previously.[51] Two different CSF batches were assayed independently by proteomics analysis, and only proteins identified in both batches were considered positive hits. The biological process classification was performed using UniProt (http://www.uniprot.org).

Data Processing. For experiments shown in Figures 3A,B, 4D,F,G, and 5B,E, the error bars represent the SD of three independent measurements. For experiments shown in Figure

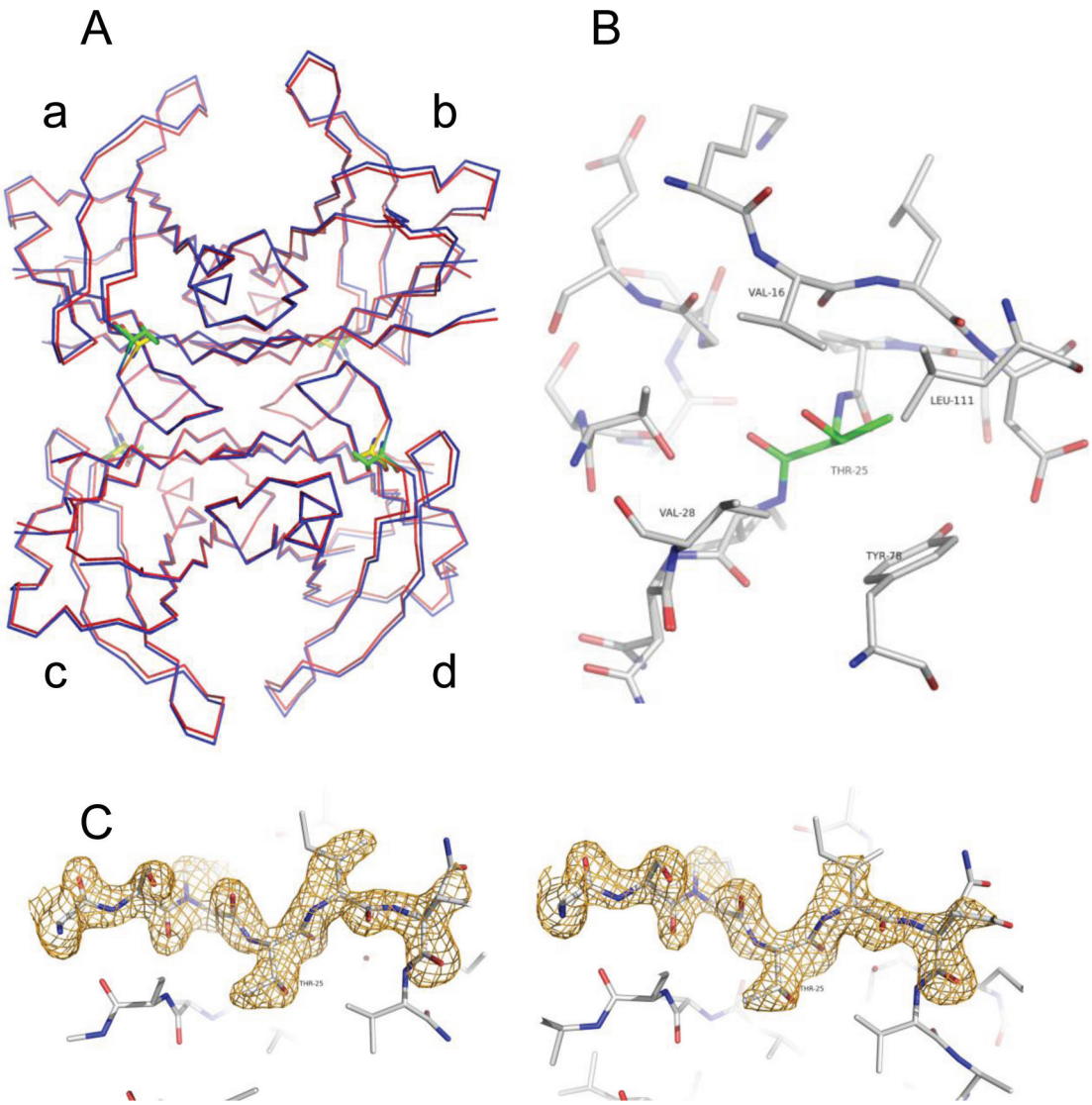

Figure 2. Comparison between the crystal structures of wt-TTR and A25T-TTR. (A) Superposition of wt-TTR (red) and A25T mutant (blue) tetramers. The alanine of the wild-type structure is colored yellow and the threonine of A25T green. The overall rmsd for the 430 superposed C_α atoms is 0.50 Å. (B) Image showing the local environment of the threonine mutation in monomer A. None of the possible rotamers for the threonine side chain (green) leads to the formation of a hydrogen bond with the γ-hydroxyl group. (C) Standard omit map ($F_{obs} - F_{calc}$ contoured at 3σ) for the region surrounding the A25T mutation (residues 21−27) in monomer A.

3C,D, the error bars represent the SD of two independent measurements. The data in Figure 3B were statistically different ($p < 0.05$; Student's t test).

For Table 3 and Table 1 of the Supporting Information, a Mascot score of >45[52] was taken as a significant threshold ($p < 0.05$). The Exponentially Modified Protein Abundance Index (emPAI)[53] offers a relative quantification of the proteins present in the proteomic experiments (Table 3 and Table 1 of the Supporting Information).

$$\text{emPAI} = 10^{N_{\text{observed}}/N_{\text{observable}}} - 1 \quad (5)$$

where N_{observed} is the number of experimentally observed peptides and $N_{\text{observable}}$ is the calculated number of observable peptides for each protein.

RESULTS AND DISCUSSION

The Structure of Homotetrameric A25T-TTR Determined Crystallographically Reveals No Substantial Structural Changes Relative to the wt-TTR Structure.

The structures of several amyloidogenic variants of TTR has been determined crystallographically, but none of these offer a clear indication of why these variants have increased amyloidogenic potential compared to that of the wt protein.[54] However, thermodynamic and kinetic studies have shown a clear decrease in tetramer stability and, in some cases, an increase in the rate of dissociation of the tetramer into monomers, explaining why the familial TTR variants are more amyloidogenic.[16−20,25,55] The highly amyloidogenic A25T-TTR variant exemplifies this correlation because its tetramer has the highest dissociation rate constant of all of the TTR variants studied thus far and is thermodynamically unstable.[16] Because the crystal structure of A25T-TTR has not yet been determined, we decided to determine its structure using X-ray crystallography to determine if, in contrast to the other TTR variants, structural defects could explain the instability and consequent amyloidogenicity of A25T-TTR.

Figure 2A shows that the overall structure of the A25T-TTR homotetramer determined to 2.03 Å resolution remains largely

dx.doi.org/10.1021/bi201365r | *Biochemistry* 2011, 50, 11070−11083

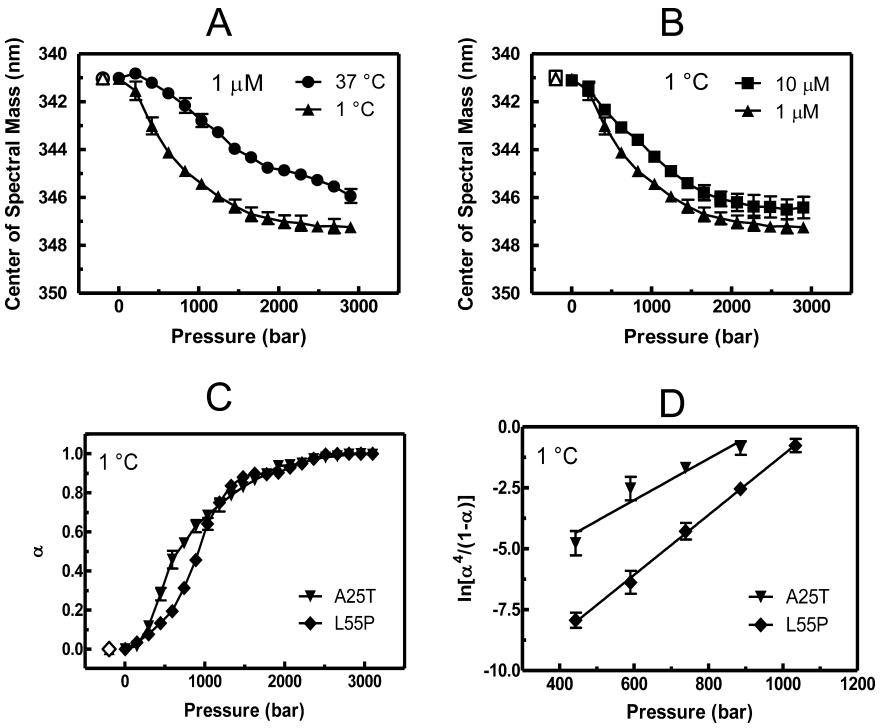

Figure 3. Tetramer of A25T-TTR that is less stable when exposed to high hydrostatic pressure than L55P-TTR, as measured by the change in the center of spectral mass of tryptophan emission. (A) The low temperature facilitates the dissociation and unfolding of A25T-TTR. The experiments were performed at pH 7.5 with 1 μM A25T-TTR at 37 (●) or 1 °C (▲). (B) The dissociation of A25T-TTR induced by high pressure has some concentration dependence at 1 °C and pH 7.5. The concentration of A25T-TTR was 1 (▲) or 10 μM (■). (C) At 1 °C and pH 7.5, A25T-TTR (▼) was less stable than L55P-TTR (◆) when exposed to high pressure. The changes in tryptophan fluorescence emission were used to calculate the extent of the reaction (α) using eq 2. (D) Plot of $\ln[\alpha^4/(1-\alpha)]$ vs pressure for A25T-TTR (▼) or L55P-TTR (◆) extracted from the data presented in panel C. From these curves, ΔV_a and ΔG_a were calculated (Table 2) from the slope and y-intercept, respectively. Empty symbols at the left of panels A–C represent the centers of spectral mass of tryptophan emission after a return to atmospheric pressure. The complete recovery of this value suggests full reversibility of the dissociation–unfolding processes. Excitation was set at 280 nm and emission collected between 300 and 400 nm.

unaltered by the A25T mutation. The root-mean-square deviation on superposition of the 460 equivalent Cα atoms of the wild-type and mutant structures was only 0.50 Å. The introduction of the threonine leads to only relatively minor perturbations of the structure, which are restricted to the vicinity of the mutation itself. The most notable difference with respect to the wt-TTR structure is a local shift in the main chain leading to a movement on the order of 0.9 Å of the Cα atom at position 25. This appears necessary for accommodation of the larger threonine side chain. The latter remains unsatisfied in terms of its hydrogen bonding valencies as its local environment provides no appropriate acceptor or donor for the side chain hydroxyl group. Rather, the environment is largely hydrophobic, composed of V16, V28, L111, and the aromatic ring of Y78 (Figure 2B), appropriate for accommodating the alanine side chain of the wild-type protein. Indeed, the electron density (Figure 2C) shows that the side chain of T25 exhibits some signs of disorder, presumably because none of the potential rotamers leads to the formation of hydrogen bonds that are expected when polar side chains are buried within the protein core.[56]

A crystallographic 2-fold axis generates the full tetrameric molecule from the two subunits [A and B (Figure 1B)] of the asymmetric unit (Figure 2A). Clearly, therefore, the A25T mutation is insufficient to perturb the stability of the native quaternary structure of TTR under the conditions used for crystallization. However, it is noteworthy that the A25T mutation lies close to the dimer–dimer interface (Figure 2A). Although the crystal structure itself provides no direct evidence of this, it seems plausible that the local perturbations described above, including the weakening of the side chain packing induced by the electrostatically unsatisfied threonine side chain, could lead to local instability of the monomeric or tetrameric structure. In solution, this may propagate to the β-hairpin, which precedes the mutation, and is part of the dimer–dimer interface. This may eventually affect the overall stability of the tetramer. Systematic urea denaturation studies conducted as a function of TTR concentration showed that tetramer dissociation and monomer unfolding equilibria are thermodynamically linked.[52] For wt-TTR, the denaturation occurs in a two-step denaturation process, tetramer to folded monomer and folded monomer to unfolded monomer.[24] The tetramers of wt-TTR dissociate first into AB and CD dimers (see Figure 2A)[11] that then dissociate into four monomers. Thus, any perturbation of the AB–CD interface might compromise A25T-TTR tetramer stability.

Pressure-Induced Dissociation of A25T-TTR: Calculating Thermodynamic Parameters for Folding and Association. Previously, we have used high hydrostatic pressure (HHP) to induce dissociation or unfolding of TTR.[17] From HHP isotherms, it is possible to calculate the change in volume and free energy of a dissociation–unfolding reaction. Sekijima and co-workers[16] have evaluated A25T-TTR stability using changes in pH to induce TTR dissociation,

partial unfolding, and aggregation; however, these processes all occur concomitantly, making it very difficult to study each process in isolation. Urea-induced unfolding has also been investigated for several variants of TTR, including A25T-TTR.[16,20,25] However, the thermodynamic parameters associated with its unfolding have not been calculated.

Our first aim was to determine whether A25T-TTR denaturation under pressure was temperature- and concentration-dependent. Pressure titration assays were performed at two different temperatures (1 and 37 °C), and structural perturbations were monitored by analyzing the changes in the center of the spectral mass of tryptophan (Trp) fluorescence emission. Each TTR monomer has two Trp residues that can be used to detect changes in the tertiary structure of the protein. As seen in Figure 3A, under pressure there was a displacement of ∼6 nm in the center of mass of Trp fluorescence emission at these two temperatures, with A25T-TTR being more sensitive to HHP-induced denaturation at the lower temperature (1 °C). The $p_{1/2}$ values (pressure that furnishes 50% of the maximum structural alterations) at 1 and 37 °C were 600 and 1400 bar, respectively. These data reinforce the role of hydrophobic interactions in maintaining the native tetrameric TTR structure.[17] The effects of pressure were completely reversible, as shown by the isolated symbols on the left of panel A. As shown in Figure 3B, the dissociation of A25T-TTR at 1 °C was somewhat dependent on concentration. With a change in protein concentration from 1 to 10 μM, there was an increase in $p_{1/2}$ from 600 ± 30 to 860 ± 58 bar [n = 3; p < 0.05; Student's t test; $\Delta p_{1/2}$ = 260 bar (Figure 3B)]. However, according to eq 4 (Experimental Procedures), the expected $\Delta p_{1/2}$ is 400 bar. This departure from the expected displacement on the pressure curve has been observed for other oligomers[57] and has been attributed to conformational heterogeneity, which increases as the number of subunits of the oligomer increases.

For the comparison of the stability of A25T-TTR to that of another unstable TTR variant, we chose L55P-TTR, which is associated with the most aggressive form of FAP.[58] At 1 °C, A25T-TTR was significantly more sensitive to pressure denaturation than L55P-TTR (Figure 3C), which had a $p_{1/2}$ value of 900 bar, 300 bar higher than that of A25T-TTR (Table 2).

Table 2. ΔG_a and ΔV_a Values for the Dissociation of A25T-TTR and L55P-TTR Tetramers at 1 °C, Calculated Using eq 3

	L55P-TTR	A25T-TTR
ΔV_a (mL/mol)	278 ± 13[a]	182 ± 39[a]
ΔG_a (kcal/mol)	−26.8 ± 0.2[a]	−23.6 ± 0.6[a]
$p_{1/2}$ (bar)	900	600

[a]Errors were calculated by statistical analysis and represent standard deviations.

From the data presented in panel C and eq 3, it is possible to calculate the changes in free energy (ΔG_a) and volume (ΔV_a) for the association and folding of A25T-TTR and L55P-TTR. The y-intercept of these curves corresponds to ΔG_a, and the slope corresponds to ΔV_a (Table 2).

As shown, A25T-TTR was less thermodynamically stable than L55P-TTR by 3 kcal/mol. Previous studies investigating the urea-induced unfolding of these variants determined $U_{1/2}$ values of 1.9 and 2.3 M for A25T-TTR and L55P-TTR, respectively,[20] suggesting that A25T-TTR is less stable the L55P-TTR. The thermodynamic stability profile of A25T-TTR denatured by urea showed that both tetramers and monomers of this variant are highly destabilized with a complicated denaturation pathway that includes formation of aggregates.[24] The ΔG_a was not calculated in these studies.[19,24] Interestingly, the ΔV_a for the dissociation of A25T-TTR was significantly lower than that observed for L55P-TTR (Table 2). The change in volume upon association was ∼100 mL/mol higher for L55P-TTR than for A25T-TTR, suggesting that the tetramers of L55P-TTR have more void volumes than the A25T-TTR tetramers. Consequently, the dissociation of this hydrated mutant should be accompanied by a smaller change in volume (Figure 3 and Table 2).

Fibrillogenesis of A25T-TTR under Physiological Conditions. Acidic pH has been frequently used as a way to trigger TTR amyloidogenesis because it induces the formation of a monomeric amyloidogenic intermediate of TTR, which is prone to aggregation.[18] However, acidic buffers are poor models for the conditions in CSF, which is where A25T-TTR undergoes fibrillogenesis. To mimic the conditions found in CSF (pH 7.3) more closely, A25T-TTR (3.5 μM) was allowed to aggregate at pH 7.3 (37 °C), and the appearance of aggregates over time was followed using size-exclusion chromatography (SEC). Wild-type TTR and L55P-TTR were used for comparison. By the second day of incubation, A25T-TTR (pH 7.3; T_2) formed higher-molecular weight species (eluting at ∼7 mL) than the A25T tetramer, which elutes at 9 mL (Figure 4A). These aggregates underwent increases in quantity and molecular mass as aggregation progressed [note the gradual shift in the peak from 7 to ∼6 mL (Figure 4A, inset)], with a concomitant decrease in the tetramer population. Even after 20 days under these aggregation-permitting conditions (T_{20}), some tetramers remained in solution (∼60%). In contrast, wt-TTR did not aggregate on this time scale under these conditions (Figure 4B), while L55P-TTR underwent minor aggregation in this environment (Figure 4C). The quantification of A25T- and L55P-TTR soluble oligomer formation as a function of time (pH 7.3) is shown in Figure 4D.

To further characterize the oligomers formed by aggregation of A25T-TTR, we took advantage of A11, an oligomer-specific antibody that does not recognize mature amyloid fibrils.[59] As shown in the inset of Figure 4D, A25T-TTR oligomers were recognized by A11 on the 11th day of incubation, no wt-TTR oligomers were detected, and only a small quantity of L55P-TTR oligomers was detected.

Native PAGE (12%) was also used to follow the aggregation of A25T-, L55P-, and wt-TTR (Figure 4E), and the tetramer population was quantified by densitometry (Figure 4F). As aggregation progresses, the magnitude of the band corresponding to the aggregated species (>270 kDa) increases with L55P-TTR (lanes 3, 6, 9, and 12) and A25T-TTR (lanes 4, 7, 10, and 13), but this increase was much more pronounced with A25T-TTR. Again, wt-TTR did not aggregate at this pH (lanes 2, 5, 8, and 11). Quantification of the disappearance of the tetramer over time confirmed the stronger tendency of A25T-TTR to undergo aggregation at neutral pH (Figure 4F). In addition to soluble oligomers, mature fibrils also formed when A25T-TTR and L55P-TTR aggregated at neutral pH, as determined by thio-T, a specific dye for amyloid fibrils. As expected, soluble A25T-TTR bound very little thio-T (Figure 4G) but, after 20

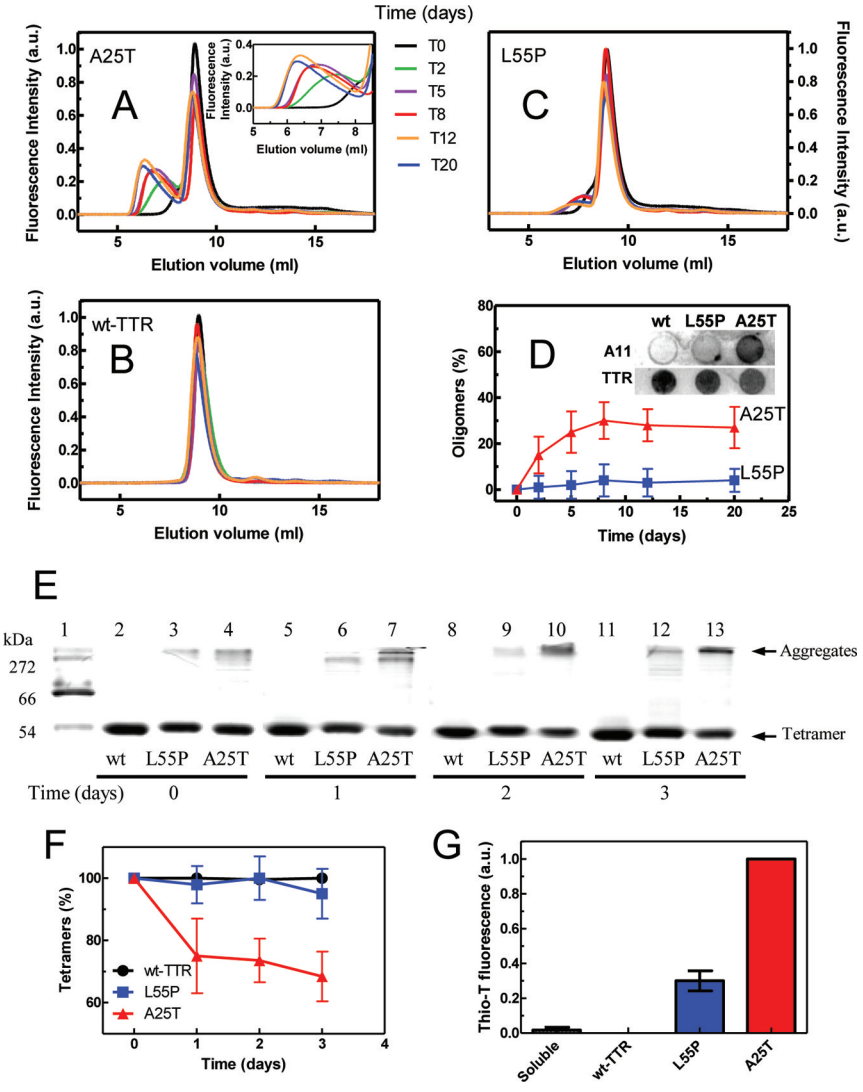

Figure 4. Aggregation kinetics of A25T-TTR, L55P-TTR, and wt-TTR at 37 °C and pH 7.3. A25T-TTR (A), wt-TTR (B), and L55P-TTR (C) (each at 3.5 μM) were incubated in PBS for 20 days at 37 °C under quiescent conditions. During this time, aliquots were withdrawn at the indicated times [day 0 (black), day 2 (green), day 5 (purple), day 8 (red), day 12 (orange), and day 20 (blue)] and injected into a gel filtration column (GPC300), and the fluorescence at 330 nm was monitored. Note that in the case of A25T-TTR, the magnitude of the peak corresponding to the tetramers (elution at 9 mL) decreased over time, while the magnitude of the peak corresponding to aggregates and/or oligomers (elution at 6−7 mL) increased. (D) Quantification of the oligomers formed during the aggregation of A25T-TTR (A) or L55P-TTR (C). The total amount of oligomers formed during the kinetic assay was quantified by calculating the total area of the peaks eluting before 9 mL. The inset of panel D shows a dot blot of A25T-TTR, wt-TTR, and L55P-TTR (3.5 μM) after incubation for 11 days in PBS at pH 7.3 and 37 °C using the A11 antibody (which recognizes prefibrillar oligomers) and an anti-TTR antibody as a loading control. (E) Time course of aggregation of 3.5 μM A25T-TTR (lanes 4, 7, 10, and 13), L55P-TTR (lanes 3, 6, 9, and 12), and wt-TTR (lanes 2, 5, 8, and 11) over 3 days at 37 °C. Aliquots were withdrawn on days 0−3 and analyzed using 12% native PAGE. Note that over time, the band corresponding to the tetramers (54 kDa) in the A25T-TTR lane decreased in intensity, with a concomitant increase in the intensity of the bands with molecular masses of >200 kDa. wt-TTR remained tetrameric, whereas L55P-TTR underwent a discrete aggregation. (F) The quantity of tetramers was estimated by densitometry of the bands at 54 kDa from panel E. (G) The aggregates of A25T-TTR and L55P-TTR formed in PBS (3.5 μM; 37 °C for 20 days) bind thioflavin T. Soluble A25T-TTR was used as a control.

days under aggregating conditions at pH 7.3, formed aggregates that were thio-T positive (Figure 4G, red bar). L55P-TTR binds 70% less thio-T than A25T-TTR (Figure 4G, blue bar), whereas wt-TTR did not produce any species that were able to bind this dye, even after incubation for 20 days at pH 7.3 (Figure 4G).

Taken together, these data suggest that A25T-TTR undergoes aggregation at pH 7.3, a pH mimicking that found in CSF, forming oligomers and amyloid fibrils (see the images of these fibrils in Figure 5C).

A25T-TTR Fibrillogenesis Takes Place in Human CSF.

Having shown that A25T-TTR is amyloidogenic in buffer at neutral pH (Figure 4), we decided to investigate whether A25T-TTR would undergo aggregation in CSF, the milieu in which this variant aggregates in LA patients. L55P-TTR was used as a control for this experiment. Aggregation of recombinant A25T- or L55P-TTR (3.5 μM) in PBS or CSF was monitored using native PAGE combined with Western blotting to quantify the disappearance of tetramers (Figure 5, panels A and B).

dx.doi.org/10.1021/bi201365r | *Biochemistry* 2011, 50, 11070−11083

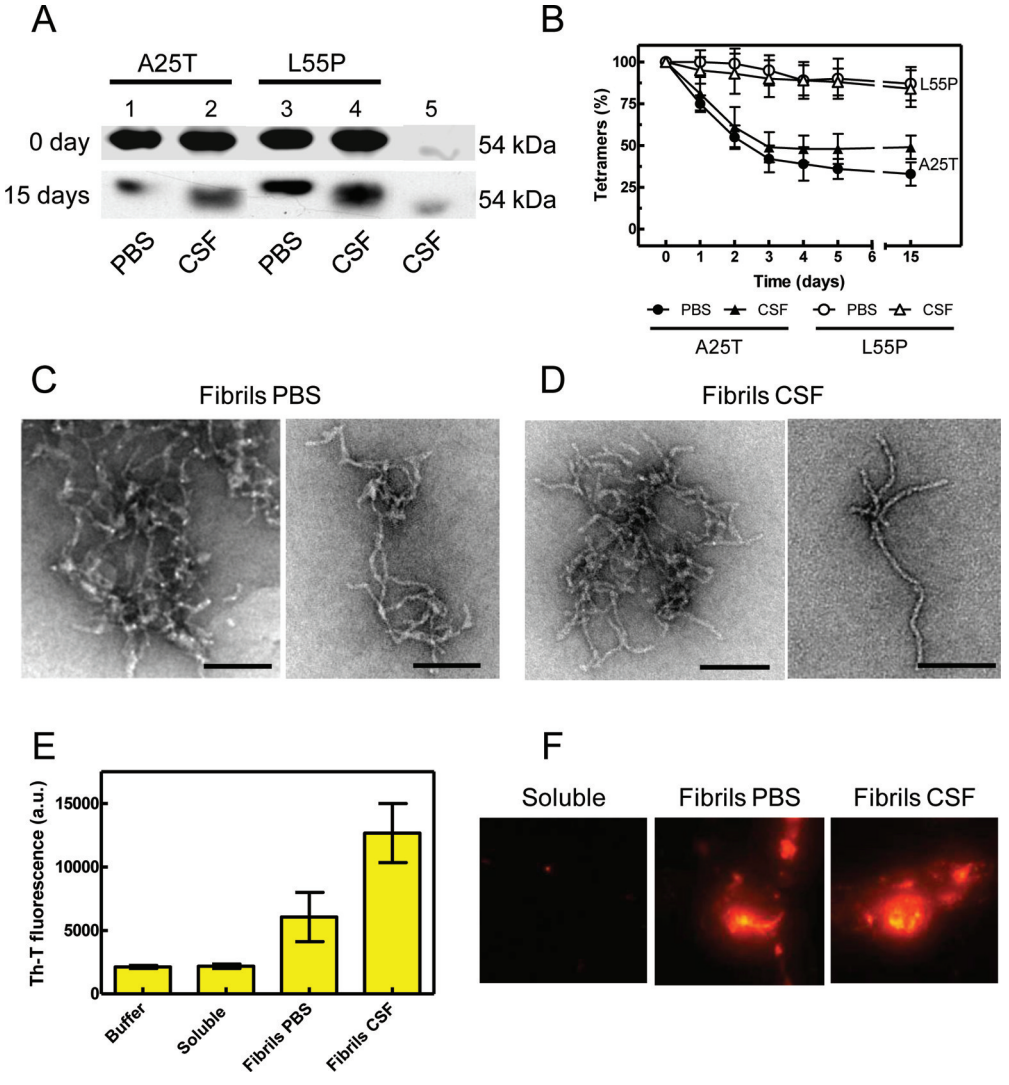

Figure 5. Evaluation of the aggregation of A25T-TTR and L55P-TTR in cerebrospinal fluid (CSF). (A) A25T-TTR (lanes 1 and 2) and L55P-TTR (lanes 3 and 4) at concentrations of 3.5 μM were allowed to aggregate in PBS (lanes 1 and 3) or CSF (lanes 2 and 4) for 15 days at 37 °C. Samples were withdrawn each day and analyzed using native PAGE and Western blotting with an anti-TTR antibody. Lane 5 shows the TTR endogenously expressed in CSF. The top gel in panel A shows a native PAGE/western blotting analysis performed immediately after the addition of 3.5 μM of each variant into PBS and CSF, showing that the amount of tetramers at time 0 is the same in all conditions. The bottom gel in panel A shows an example of the band corresponding to the tetramer after incubation for 15 days at 37 °C. Note that there was a marked decrease in the tetramer population, especially in the case of A25T-TTR. (B) Quantification by densitometry of the band corresponding to the tetramers during the formation of A25T-TTR and L55P-TTR aggregates. That raw data are for day 15 only. Electron microscopy images of pelleted A25T-TTR fibrils aged for 15 days at 37 °C at PBS (C) or CSF (D). The scale bar is 100 nm. (E) Thioflavin T fluorescence (20 μM) of the fibrils presented in panels C and D (protein concentration of 45 μg/mL). As controls, soluble A25T-TTR (45 μg/mL) and buffer without protein were used. (F) Fluorescence emission imaging of Congo red (10 μM) bound to the aggregates of A25T-TTR formed in PBS or CSF. The first panel shows the emission of Congo red in the presence of soluble protein (negative control). Images are shown at 2000× magnification.

Before aggregation (day 0), there are equal amounts of A25T-TTR (Figure 5A, lanes 1 and 2) and L55P-TTR (lanes 3 and 4) in PBS and CSF, as measured using a TTR-specific antibody (54 kDa band). As expected, CSF had a small amount of endogenous TTR (Figure 5A, lane 5). The samples were then incubated at 37 °C without agitation, and aliquots were withdrawn daily and assayed using native PAGE. The gel shown in the bottom panel of Figure 5A illustrates the profile after incubation for 15 days under these conditions. The population of A25T-TTR tetramers (54 kDa band) decreased considerably over time (Figure 5B); this effect was not observed with L55P-TTR, whose tetramer population decreased by only ~15%. Aggregation of A25T-TTR was equally effective in the two pH-neutral environments investigated here, which differ in their compositional complexity.

To verify the nature of the A25T-TTR aggregates in PBS or CSF, the samples were pelleted and the pellets were analyzed by electron microscopy (EM), thio-T fluorescence, and Congo red binding. EM analysis of A25T-TTR aggregates after aggregation for 15 days in PBS or CSF (panel C or D of Figure 5, respectively) showed a typical amyloid pattern in both samples. These aggregates were able to bind thio-T (Figure 5E) and exhibit Congo red binding (Figure 5F), confirming their amyloid characteristic. As far as we know, this is the first image of an aggregate of TTR generated in vitro in an environment that closely models its physiological setting.

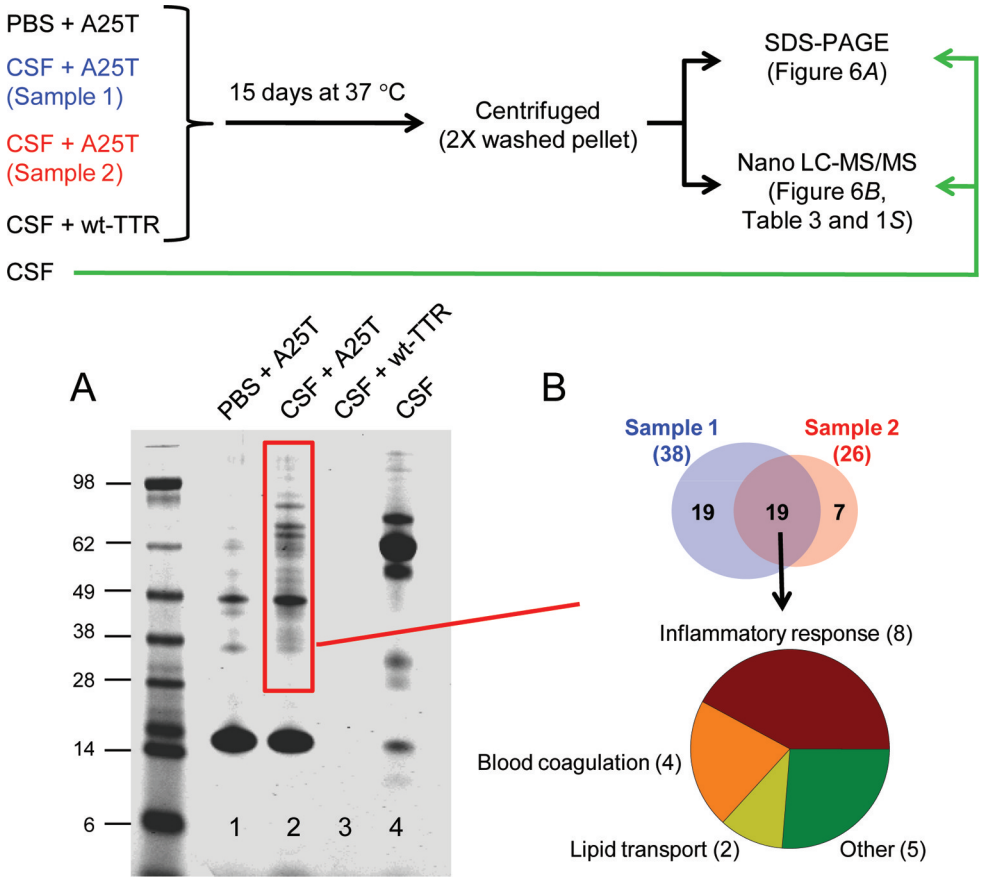

Figure 6. Aggregates of A25T-TTR in human CSF bind several endogenous proteins. Identification by proteomics analysis. On top: Design of proteomics experiments to identify by LC−MS/MS CSF proteins copurified with A25T-TTR during amyloid aggregation. (A) SDS−PAGE of 3.5 μM A25T-TTR incubated at 37 °C for 15 days in PBS (lane 1) or CSF (lanes 2). After this period, the samples were washed twice to remove nonspecifically bound proteins, and the pellets were applied to the gel (A) or subjected to LC−MS/MS (B). As a control, CSF (lane 3) with 3.5 μM wt-TTR was incubated under the same condition to determine if the endogenous proteins alone or with wt-TTR undergo aggregation. Soluble CSF (lane 4) was also used as a control. (B) Overlap between the proteins identified in samples 1 and 2. Total numbers of identified proteins are given in parentheses. Below is the proteomic profile of 19 proteins identified in samples 1 and 2 (for details, see Table 3).

The Aggregates of A25T-TTR Formed in CSF Bind Several Proteins. Amyloid deposits formed in vivo are composed mostly of a single protein, but a variety of other proteins, such as serum amyloid P, are often associated with the amyloid fibrils.[60] These amyloid fibril-associated proteins commonly result in enhanced fibril resistance to immune defense mechanisms or to protease degradation.[60] To evaluate whether A25T-TTR aggregates bound other proteins from human CSF, recombinant A25T-TTR was added to human CSF and incubated for 15 days at 37 °C. The samples were then centrifuged to collect the aggregates, washed twice to remove any loosely bound proteins, and analyzed by SDS−PAGE (sample preparation scheme at the top of Figure 6).

When aggregation was performed in PBS (Figure 6A, lane 1), TTR existed mostly as a monomer after SDS boiling of the fibrils that are sensitive to SDS, but there were also other visible bands, one with a molecular mass of approximately 50 kDa suggesting the presence of SDS-resistant tetramers. Interestingly, when aggregation was performed in CSF (Figure 6A, lane 2), a variety of additional proteins were bound to, and coprecipitated with, the A25T-TTR amyloid fibrils. It is important to note that these aggregates are typical amyloid fibrils as observed by EM, as well as thio-T and Congo red binding (Figure 5C−F). As a control, a solution of recombinant wt-TTR (3.5 μM) was incubated in human CSF for 15 days at 37 °C (Figure 6A, lane 3). The absence of proteins in this lane indicates that neither the endogenous proteins present in CSF nor wt-TTR demonstrated a tendency to aggregate under these conditions. Collectively, these experiments suggest that the aggregates formed in CSF are composed of exogenous A25T-TTR, which binds several proteins present in this complex environment. To determine whether A25T-TTR amyloidogenesis is driven by these protein interactions in the CSF or whether the associated proteins are brought down as ligands to the amyloid fibrils, A25T-TTR amyloid fibrils preformed in PBS for 15 days at 37 °C (Figure 5C) were pelleted and incubated for an additional 15 days in CSF at 37 °C. The preformed fibrils of A25T-TTR recruited far fewer CSF proteins when compared to A25T-TTR fibrils produced in the CSF (data not shown). This result suggests that proteins from CSF associate with A25T-TTR both during the aggregation process and after the formation of mature amyloid fibrils.

Next, we used a proteomics methodology to identify the proteins that co-aggregate with A25T-TTR amyloid fibrils. For this purpose, we submitted two independent batches of A25T-TTR amyloid fibrils aged for 15 days in CSF to nano LC−MS/MS proteomics analysis (scheme at the top of Figure 6). To ensure that the proteins identified were from human CSF and not a contaminant present in the A25T-TTR recombinant

Table 3. Characterization by LC−MS/MS of Proteins Copurified with A25T-TTR Amyloid Fibrils[a]

accession code	protein	gene name	biological process	no. of observed peptides[b]	Mascot score[b]	emPAI[b,c]
AAA85332.1	complement C3	C3	inflammatory response/ complement pathway	23/8	1575/556	0.72/0.26
AAA51x55.1	complement C4-A	C4A	inflammatory response/ complement pathway	15/3	1044/219	0.32/0.06
P02746	complement C1q subcomponent subunit B	C1QB	inflammatory response/ complement pathway	1/3	50/143	0.14/0.51
BAA86864.1	complement C1s subcomponent	C1S	inflammatory response/ complement pathway	2/1	123/53	0.21/0.14
P01857	Ig γ-1 chain C region	IGHG1	Inflammatory response	2/7	98/446	0.20/0.64
B45874	Ig α-1 chain C region	IGHA1	inflammatory response	2/2	111/111	0.20/0.20
CAA67886.1	Ig γ-3 chain C region	IGHG3	inflammatory response	2/5	104/308	0.20/0.66
CAA29999.1	monocyte differentiation antigen CD14	CD14	inflammatory response	1/1	65/65	0.09/0.09
AAA51765.1	clusterin	CLU	apoptosis/inflammatory response	1/1	82/81	0.08/0.08
NP_000884.1	kininogen-1	KNG1	blood coagulation/inflammatory response	3/1	195/59	0.34/0.08
AAA52429.1	fibrinogen β chain	FGB	blood coagulation	4/6	273/356	0.30/0.48
AAB59531.1	fibrinogen γ chain	FGG	blood coagulation	1/1	66/66	0.07/0.07
1ATH_A	antithrombin-III	SERPINC1	blood coagulation	1/1	62/62	0.08/0.08
AAV38664.1	apolipoprotein D	APOD	lipid transport	2/1	150/81	0.82/0.13
1H7I_A	apolipoprotein E	APOE	lipid transport	4/1	280/75	0.59/0.20
NP_001034438.1	EGF-containing fibulin-like extracellular matrix protein 1	EFEMP1	peptidyl-tyrosine phosphorylation	8/4	522/280	0.66/0.38
AAK37822.1	fibulin-1	FBLN1	host−virus interaction	11/2	785/191	0.71/0.12
CAA45026.1	actin, cytoplasmic 1	ACTB	adherents junction organization	1/1	97/77	0.09/0.09
BAA08084.1	ceruloplasmin	CP	oxidation−reduction process	3/1	153/60	0.12/0.04

[a]Significance threshold of $p < 0.05$ (Mascot score of >45). [b]Sample 1/sample 2. [c]Exponentially Modified Protein Abundance Index (emPAI).

protein, we applied the same protocol to A25T-TTR fibrils produced in PBS. As expected, we identified only TTR by LC−MS/MS in the fibrils formed in PBS. For the A25T-TTR fibrils aged in CSF, 19 amyloid-associated proteins were common to both CSF samples (Figure 6B and Table 3). All 19 of the A25T-TTR amyloid-associated proteins are found naturally in human CSF samples, as confirmed by our CSF proteomic analysis (Table 1 of the Supporting Information) or by previous reports.[61]

Among the CSF proteins identified, clusterin, apolipoprotein E, and actin have been previously associated with many other amyloids, including transthyretin amyloid fibrils.[50,62−64] Complement proteins have also been shown to be associated with amyloid fibrils. We found not only complement proteins (C3, C4A, C1qB, and C1s) but also immunoglobulins (IGHG1, JGHA1, and IGHG3) associated with A25T-TTR fibrils, suggesting activation of the immune system upon TTR amyloid formation. Fibrinogen has also been found in amyloid plaques from patients with Alzheimer's disease.[65] Besides fibrinogen, we detected kininogen-1 and antithrombin-III, suggesting a possible link between A25T-TTR fibrillogenesis and the blood coagulation cascade in the CSF. A connection between perturbations of the coagulation and fibrinolytic systems and the process of amyloidogenesis has been suggested previously.[66] Recruitment of proteins associated with blood hemostasis to A25T-TTR amyloid fibrils may be useful in explaining the micro bleeds and subarachnoid hemorrhages integral to LA pathology.[67] The relevance of fibulin-1, EGF-containing fibulin-like extracellular, monocyte differentiation antigen CD14, and ceruloplasmin to LA development may be addressed in the future.

CONCLUSIONS

The results of this study quantitatively confirm that A25T-TTR is highly amyloidogenic and forms amyloid fibrils in CSF. The protein molecules associated with the A25T-TTR amyloid fibrils are highly complex and diverse, implicating the disruption of many cellular and extracellular physiological pathways, which may play a role in disease development depending on the extent of perturbation. This complexity is also present in intracellular protein aggregates, as published recently by the groups of Vabulas and Hartl.[68] In this case, the loss of function of the recruited proteins was proposed as a possible explanation for the toxicity of amyloid aggregates, a hypothesis that should also be considered in LA. The data described herein prompt new questions. Are the co-aggregated proteins identified here specific for the aggregation of A25T-TTR? What is the contribution of these partners to fibril stability and clearance? We believe that these are some of the important questions that should be addressed in the future. The success achieved here in tracking the aggregation of TTR in CSF opens several new avenues of investigation, such as the screening of possible inhibitors of fibrillogenesis in a more relevant environment for LA or FAP.[69]

ASSOCIATED CONTENT

Supporting Information

Complete proteomic characterization of A25T-TTR amyloid fibrils formed in CSF (samples 1 and 2) and the CSF used in this work (Table 1). This material is available free of charge via the Internet at http://pubs.acs.org.

Accession Codes

The atomic coordinates have been deposited in the Protein Data Bank as entry 3TFB.

AUTHOR INFORMATION

Corresponding Author

*F.L.P.: e-mail, palhano@bioqmed.ufrj.br. D.F.: e-mail, foguel@bioqmed.ufrj.br; phone, (55-21) 2562-6761; fax, (55-21) 2270-8647.

Funding

This work was supported by grants from Conselho Nacional de Desenvolvimento Científico e Tecnológico (CNPq), Fundação Carlos Chagas Filho de Amparo à Pesquisa do Estado do Rio de Janeiro (FAPERJ), and Coordenação de Aperfeiçoamento de Pessoal de Nível Superior (CAPES).

ACKNOWLEDGMENTS

We are very grateful to Emerson R. Gonçalves for competent technical assistance. We thank Colleen Fearns for help with preparation of the manuscript and Lisa Ryno for help with the graphic for the table of contents. We also thank Dr. Evan Powers for help with the statistical analyses. This work is dedicated to Dr. Martha M. Sorenson who has reviewed with outstanding scientific criticism hundreds of manuscripts produced by the researchers of Instituto de Bioquímica Médica, Universidade Federal do Rio de Janeiro, over the past 27 years.

ABBREVIATIONS

CSF, cerebrospinal fluid; CNS, central nervous system; CNSA, central nervous system amyloidosis; CR, Congo red; FAC, familial amyloidotic cardiomyopathy; FAP, familial amyloidotic polyneuropathy; HHP, high hydrostatic pressure; LA, leptomeningeal amyloidosis; rmsd, root-mean-square deviation; SDS−PAGE, sodium dodecyl sulfate−polyacrylamide gel electrophoresis; TTR, transthyretin; T4, thyroxine.

REFERENCES

(1) Chiti, F., and Dobson, C. M. (2006) Protein misfolding, functional amyloid, and human disease. *Annu. Rev. Biochem. 75*, 333−366.

(2) Colon, W., and Kelly, J. W. (1992) Partial denaturation of transthyretin is sufficient for amyloid fibril formation in vitro. *Biochemistry 31*, 8654−8660.

(3) Sipe, J. D., Benson, M. D., Buxbaum, J. N., Ikeda, S., Merlini, G., Saraiva, M. J., and Westermark, P. (2010) Amyloid fibril protein nomenclature: 2010 recommendations from the nomenclature committee of the International Society of Amyloidosis. *Amyloid 17*, 101−104.

(4) Luhrs, T., Ritter, C., Adrian, M., Riek-Loher, D., Bohrmann, B., Dobeli, H., Schubert, D., and Riek, R. (2005) 3D structure of Alzheimer's amyloid-β(1−42) fibrils. *Proc. Natl. Acad. Sci. U.S.A. 102*, 17342−17347.

(5) Petkova, A. T., Ishii, Y., Balbach, J. J., Antzutkin, O. N., Leapman, R. D., Delaglio, F., and Tycko, R. (2002) A structural model for Alzheimer's β-amyloid fibrils based on experimental constraints from solid state NMR. *Proc. Natl. Acad. Sci. U.S.A. 99*, 16742−16747.

(6) Nelson, R., Sawaya, M. R., Balbirnie, M., Madsen, A. O., Riekel, C., Grothe, R., and Eisenberg, D. (2005) Structure of the cross-β spine of amyloid-like fibrils. *Nature 435*, 773−778.

(7) Wasmer, C., Lange, A., Van Melckebeke, H., Siemer, A. B., Riek, R., and Meier, B. H. (2008) Amyloid fibrils of the HET-s(218−289) prion form a β solenoid with a triangular hydrophobic core. *Science 319*, 1523−1526.

(8) Dobson, C. M. (2003) Protein folding and misfolding. *Nature 426*, 884−890.

(9) Guijarro, J. I., Sunde, M., Jones, J. A., Campbell, I. D., and Dobson, C. M. (1998) Amyloid fibril formation by an SH3 domain. *Proc. Natl. Acad. Sci. U.S.A. 95*, 4224−4228.

(10) Hamilton, J. A., and Benson, M. D. (2001) Transthyretin: A review from a structural perspective. *Cell. Mol. Life Sci. 58*, 1491−1521.

(11) Foss, T. R., Wiseman, R. L., and Kelly, J. W. (2005) The Pathway by Which the Tetrameric Protein Transthyretin Dissociates. *Biochemistry 44*, 15525−15533.

(12) Monaco, H. L., Rizzi, M., and Coda, A. (1995) Structure of a complex of two plasma proteins: Transthyretin and retinol-binding protein. *Science 268*, 1039−1041.

(13) Schreiber, G., Southwell, B. R., and Richardson, S. J. (1995) Hormone delivery systems to the brain-transthyretin. *Exp. Clin. Endocrinol. Diabetes 103*, 75−80.

(14) Westermark, P., Sletten, K., Johansson, B., and Cornwell, G. G. (1990) Fibril in senile systemic amyloidosis is derived from normal transthyretin. *Proc. Natl. Acad. Sci. U.S.A. 87*, 2843−2845.

(15) Connors, L. H., Lim, A., Prokaeva, T., Roskens, V. A., and Costello, C. E. (2003) Tabulation of human transthyretin (TTR) variants, 2003. *Amyloid 10*, 160−184.

(16) Sekijima, Y., Hammarstrom, P., Matsumura, M., Shimizu, Y., Iwata, M., Tokuda, T., Ikeda, S., and Kelly, J. W. (2003) Energetic characteristics of the new transthyretin variant A25T may explain its atypical central nervous system pathology. *Lab. Invest. 83*, 409−417.

(17) Ferrao-Gonzales, A. D., Palmieri, L., Valory, M., Silva, J. L., Lashuel, H., Kelly, J. W., and Foguel, D. (2003) Hydration and packing are crucial to amyloidogenesis as revealed by pressure studies on transthyretin variants that either protect or worsen amyloid disease. *J. Mol. Biol. 328*, 963−974.

(18) McCutchen, S. L., Lai, Z., Miroy, G., Kelly, J. W., and Colon, W. (1995) Comparison of lethal and non-lethal transthyretin variants and their relationship to amyloid disease. *Biochemistry 34*, 13527−13536.

(19) Quintas, A., Saraiva, M. J. M., and Brito, R. M. M. (1999) The tetrameric protein transthyretin dissociates to a non-native monomer in solution. A novel model for amyloidogenesis. *J. Biol. Chem. 274*, 32943−32949.

(20) Sekijima, Y., Wiseman, R. L., Matteson, J., Hammarstrom, P., Miller, S. R., Sawkar, A. R., Balch, W. E., and Kelly, J. W. (2005) The biological and chemical basis for tissue-selective amyloid disease. *Cell 121*, 73−85.

(21) Hurshman, A. R., White, J. T., Powers, E. T., and Kelly, J. W. (2004) Transthyretin aggregation under partially denaturing conditions is a downhill polymerization. *Biochemistry 43*, 7365−7381.

(22) Kelly, J. W., Colon, W., Lai, Z., Lashuel, H. A., McCulloch, J., McCutchen, S. L., Miroy, G. J., and Peterson, S. A. (1997) Transthyretin quaternary and tertiary structural changes facilitate misassembly into amyloid. *Adv. Protein Chem. 50*, 161−181.

(23) Lai, Z., Colon, W., and Kelly, J. W. (1996) The Acid-Mediated Denaturation Pathway of Transthyretin Yields a Conformational Intermediate Which Can Self-Assemble into Amyloid. *Biochemistry 35*, 6470−6482.

(24) McCutchen, S., Colon, W., and Kelly, J. W. (1993) Transthyretin mutation Leu-55-Pro significantly alters tetramer stability and increases amyloidogenicity. *Biochemistry 32*, 12119−12127.

(25) Hurshman Babbes, A. R., Powers, E. T., and Kelly, J. W. (2008) Quantification of the thermodynamically linked quaternary and tertiary structural stabilities of transthyretin and its disease-associated variants: The relationship between stability and amyloidosis. *Biochemistry 47*, 6969−6984.

(26) Liu, K., Cho, H. S., Lashuel, H. A., Kelly, J. W., and Wemmer, D. E. (2000) A glimpse of a possible amyloidogenic intermediate of transthyretin. *Nat. Struct. Biol. 7*, 754−757.

(27) Serag, A. A., Altenbach, C., Gingery, M., Hubbell, W. L., and Yeates, T. O. (2002) Arrangement of subunits and ordering of β-strands in an amyloid sheet. *Nat. Struct. Biol. 9*, 734−739.

(28) Olofsson, A., Ippel, J. H., Wijmenga, S. S., Lundgren, E., and Ohman, A. (2004) Probing solvent accessibility of transthyretin amyloid by solution NMR spectroscopy. *J. Biol. Chem. 279*, 5699−5707.

(29) Palmieri Lde, C., Lima, L. M., Freire, J. B., Bleicher, L., Polikarpov, I., Almeida, F. C., and Foguel, D. (2010) Novel Zn^{2+}-

binding sites in human transthyretin: Implications for amyloidogenesis and retinol-binding protein recognition. *J. Biol. Chem. 285*, 31731–31741.
(30) Wilkinson-White, L. E., and Easterbrook-Smith, S. B. (2007) Characterization of the binding of Cu(II) and Zn(II) to transthyretin: Effects on amyloid formation. *Biochemistry 46*, 9123–9132.
(31) Cardoso, I., Almeida, M. R., Ferreira, N., Arsequell, G., Valencia, G., and Saraiva, M. J. (2007) Comparative in vitro and ex vivo activities of selected inhibitors of transthyretin aggregation: Relevance in drug design. *Biochem. J. 408*, 131–138.
(32) Ando, Y. (2005) Liver transplantation and new therapeutic approaches for familial amyloidotic polyneuropathy (FAP). *Med. Mol. Morphol. 38*, 142–154.
(33) Liepnieks, J. J., and Benson, M. D. (2007) Progression of cardiac amyloid deposition in hereditary transthyretin amyloidosis patients after liver transplantation. *Amyloid 14*, 277–282.
(34) Yazaki, M., Mitsuhashi, S., Tokuda, T., Kametani, F., Takei, Y. I., Koyama, J., Kawamorita, A., Kanno, H., and Ikeda, S. I. (2007) Progressive wild-type transthyretin deposition after liver transplantation preferentially occurs onto myocardium in FAP patients. *Am. J. Transplant. 7*, 235–242.
(35) Lauro, A., Diago Uso, T., Masetti, M., Di Benedetto, F., Cautero, N., De Ruvo, N., Dazzi, A., Quintini, C., Begliomini, B., Siniscalchi, A., Ramacciato, G., Risaliti, A., Miller, C. M., and Pinna, A. D. (2005) Liver transplantation for familial amyloid polyneuropathy non-VAL30MET variants: Are cardiac complications influenced by prophylactic pacing and immunosuppressive weaning? *Transplant. Proc. 37*, 2214–2220.
(36) Miroy, G. J., Lai, Z., Lashuel, H., Peterson, S. A., Strang, C., and Kelly, J. W. (1996) Inhibiting Transthyretin Amyloid Fibril Formation via Protein Stabilization. *Proc. Natl. Acad. Sci. U.S.A. 93*, 15051–15056.
(37) Almeida, M. R., Gales, L., Damas, A. M., Cardoso, I., and Saraiva, M. J. (2005) Small transthyretin (TTR) ligands as possible therapeutic agents in TTR amyloidoses. *Curr. Drug Targets: CNS Neurol. Disord. 4*, 587–596.
(38) Sekijima, Y., Kelly, J. W., and Ikeda, S.-i. (2008) Pathogenesis of and therapeutic strategies to ameliorate the transthyretin amyloidoses. *Curr. Pharm. Des. 14*, 3219–3230.
(39) Johnson, S. M., Wiseman, R. L., Sekijima, Y., Green, N. S., Adamski-Werner, S. L., and Kelly, J. W. (2005) Native State Kinetic Stabilization as a Strategy To Ameliorate Protein Misfolding Diseases: A Focus on the Transthyretin Amyloidoses. *Acc. Chem. Res. 38*, 911–921.
(40) Sekijima, Y., Dendle Maria, A., and Kelly Jeffery, W. (2006) Orally administered diflunisal stabilizes transthyretin against dissociation required for amyloidogenesis. *Amyloid 13*, 236–249.
(41) Lashuel, H. A., Wurth, C., Woo, L., and Kelly, J. W. (1999) The Most Pathogenic Transthyretin Variant, L55P, Forms Amyloid Fibrils under Acidic Conditions and Protofilaments under Physiological Conditions. *Biochemistry 38*, 13560–13573.
(42) Silva, J. L., Foguel, D., and Royer, C. A. (2001) Pressure provides new insights into protein folding, dynamics and structure. *Trends Biochem. Sci. 26*, 612–618.
(43) Paladini, A. A. Jr., and Weber, G. (1981) Pressure-induced reversible dissociation of enolase. *Biochemistry 20*, 2587–2593.
(44) Kabsch, W. (2010) Xds. *Acta Crystallogr. D66*, 125–132.
(45) McCoy, A. J. (2007) Solving structures of protein complexes by molecular replacement with Phaser. *Acta Crystallogr. D63*, 32–41.
(46) Adams, P. D., Grosse-Kunstleve, R. W., Hung, L. W., Ioerger, T. R., McCoy, A. J., Moriarty, N. W., Read, R. J., Sacchettini, J. C., Sauter, N. K., and Terwilliger, T. C. (2002) PHENIX: Building new software for automated crystallographic structure determination. *Acta Crystallogr. D58*, 1948–1954.
(47) Emsley, P., and Cowtan, K. (2004) Coot: Model-building tools for molecular graphics. *Acta Crystallogr. D60*, 2126–2132.
(48) Laskowski, R. A., MacArthur, M. W., Moss, D. S., and Thornton, J. M. (1993) PROCHECK: A program to check the stereochemical quality of protein structures. *J. Appl. Crystallogr. 26*, 283–291.
(49) Davis, I. W., Leaver-Fay, A., Chen, V. B., Block, J. N., Kapral, G. J., Wang, X., Murray, L. W., Arendall, W. B. III, Snoeyink, J., Richardson, J. S., and Richardson, D. C. (2007) MolProbity: All-atom contacts and structure validation for proteins and nucleic acids. *Nucleic Acids Res. 35*, W375–W383.
(50) Murphy, C. L., Wang, S., Williams, T., Weiss, D. T., and Solomon, A. (2006) Characterization of systemic amyloid deposits by mass spectrometry. *Methods Enzymol. 412*, 48–62.
(51) Pendyala, G., Trauger, S. A., Kalisiak, E., Ellis, R. J., Siuzdak, G., and Fox, H. S. (2009) Cerebrospinal fluid proteomics reveals potential pathogenic changes in the brains of SIV-infected monkeys. *J. Proteome Res. 8*, 2253–2260.
(52) Cooper, B. (2011) The problem with peptide presumption and low Mascot scoring. *J. Proteome Res. 10*, 1432–1435.
(53) Ishihama, Y., Oda, Y., Tabata, T., Sato, T., Nagasu, T., Rappsilber, J., and Mann, M. (2005) Exponentially modified protein abundance index (emPAI) for estimation of absolute protein amount in proteomics by the number of sequenced peptides per protein. *Mol. Cell. Proteomics 4*, 1265–1272.
(54) Hornberg, A., Eneqvist, T., Olofsson, A., Lundgren, E., and Sauer-Eriksson, A. E. (2000) A Comparative Analysis of 23 Structures of the Amyloidogenic Protein Transthyretin. *J. Mol. Biol. 302*, 649–669.
(55) Hammarstrom, P., Jiang, X., Hurshman, A. R., Powers, E. T., and Kelly, J. W. (2002) Sequence-dependent denaturation energetics: A major determinant in amyloid disease diversity. *Proc. Natl. Acad. Sci. U.S.A. 99* (Suppl. 4), 16427–16432.
(56) Baker, E. N., and Hubbard, R. E. (1984) Hydrogen bonding in globular proteins. *Prog. Biophys. Mol. Biol. 44*, 97–179.
(57) Silva, J. L., and Weber, G. (1993) Pressure stability of proteins. *Annu. Rev. Phys. Chem. 44*, 89–113.
(58) Sebastiao, M. P., Saraiva, M. J., and Damas, A. M. (1998) The crystal structure of amyloidogenic Leu55 → Pro transthyretin variant reveals a possible pathway for transthyretin polymerization into amyloid fibrils. *J. Biol. Chem. 273*, 24715–24722.
(59) Kayed, R., Head, E., Thompson, J. L., McIntire, T. M., Milton, S. C., Cotman, C. W., and Glabe, C. G. (2003) Common structure of soluble amyloid oligomers implies common mechanism of pathogenesis. *Science 300*, 486–489.
(60) Pepys, M. B. (2006) Amyloidosis. *Annu. Rev. Med. 57*, 223–241.
(61) Zougman, A., Pilch, B., Podtelejnikov, A., Kiehntopf, M., Schnabel, C., Kumar, C., and Mann, M. (2008) Integrated analysis of the cerebrospinal fluid peptidome and proteome. *J. Proteome Res. 7*, 386–399.
(62) Lee, K. W., Lee, D. H., Son, H., Kim, Y. S., Park, J. Y., Roh, G. S., Kim, H. J., Kang, S. S., Cho, G. J., and Choi, W. S. (2009) Clusterin regulates transthyretin amyloidosis. *Biochem. Biophys. Res. Commun. 388*, 256–260.
(63) Greene, M. J., Sam, F., Soo Hoo, P. T., Patel, R. S., Seldin, D. C., and Connors, L. H. (2011) Evidence for a functional role of the molecular chaperone clusterin in amyloidotic cardiomyopathy. *Am. J. Pathol. 178*, 61–68.
(64) Klein, C. J., Vrana, J. A., Theis, J. D., Dyck, P. J., Spinner, R. J., Mauermann, M. L., Bergen, H. R. III, Zeldenrust, S. R., and Dogan, A. (2011) Mass spectrometric-based proteomic analysis of amyloid neuropathy type in nerve tissue. *Arch. Neurol. 68*, 195–199.
(65) Liao, L., Cheng, D., Wang, J., Duong, D. M., Losik, T. G., Gearing, M., Rees, H. D., Lah, J. J., Levey, A. I., and Peng, J. (2004) Proteomic characterization of postmortem amyloid plaques isolated by laser capture microdissection. *J. Biol. Chem. 279*, 37061–37068.
(66) Hammarstrom, P. (2007) The bloody path of amyloids and prions. *J. Thromb. Haemostasis 5*, 1136–1138.
(67) Robbins, M. S., and Yasen, J. (2008) Extensive intracranial microbleeds in transthyretin amyloidosis. *J. Am. Geriatr. Soc. 56*, 1966–1967.
(68) Olzscha, H., Schermann, S. M., Woerner, A. C., Pinkert, S., Hecht, M. H., Tartaglia, G. G., Vendruscolo, M., Hayer-Hartl, M., Hartl, F. U., and Vabulas, R. M. (2011) Amyloid-like aggregates

sequester numerous metastable proteins with essential cellular functions. *Cell 144*, 67−78.
(69) Choi, S., and Kelly, J. W. (2011) A competition assay to identify amyloidogenesis inhibitors by monitoring the fluorescence emitted by the covalent attachment of a stilbene derivative to transthyretin. *Bioorg. Med. Chem. 19*, 1505−1514.